J Biol Inorg Chem (2006) 11: 351–358
DOI 10.1007/s00775-006-0083-z

ORIGINAL PAPER

Alison Costello · Gopalraj Periyannan
Ke-Wu Yang · Michael W. Crowder · David L. Tierney

Site-selective binding of Zn(II) to metallo-β-lactamase L1 from *Stenotrophomonas maltophilia*

Received: 16 November 2005 / Accepted: 20 January 2006 / Published online: 18 February 2006

Abstract Extended X-ray absorption fine structure studies of the metallo-β-lactamase L1 from *Stenotrophomonas maltophilia* containing 1 and 2 equiv of Zn(II) and containing 2 equiv of Zn(II) plus hydrolyzed nitrocefin are presented. The data indicate that the first, catalytically dominant metal ion is bound by L1 at the consensus Zn_1 site. The data further suggest that binding of the first metal helps preorganize the ligands for binding of the second metal ion. The di-Zn enzyme displays a well-defined metal–metal interaction at 3.42 Å. Reaction with the β-lactam antibiotic nitrocefin results in a product-bound species, in which the ring-opened lactam rotates in the active site to present the S1 sulfur atom of nitrocefin to one of the metal ions for coordination. The product bridges the two metal ions, with a concomitant lengthening of the Zn–Zn interaction to 3.62 Å.

Keywords Extended X-ray absorption fine structure · Metallo-β-lactamase · L1

Introduction

Metallo-β-lactamases (MβLs) are enzymes that hydrolyze and inactivate β-lactam containing antibiotics, rendering bacteria resistant to the largest class of antibiotics [1–4]. MβLs are found in an increasing number of pathogenic bacteria, including *Bacillus anthracis* [5] and *Pseudomonas aeruginosa* [6], and there is concern for the spread of MβLs to more pathogenic organisms. A large number of structural, mechanistic, and computational studies on various MβLs have been reported [7–34]. However, some significant questions remain regarding these enzymes. For many examples, the physiologically relevant metal content has not been unambiguously established.

All MβLs are isolated containing 1–2 equivof Zn(II) [3, 35], and all of the enzymes except those from *Aeromonas* species require two Zn(II)s for full activity [36, 37]. Nonetheless, Wommer et al. [38] recently hypothesized that all of the MβLs are metal-free in vivo and bind one Zn(II) only in the presence of substrate. In contrast, Periyannan et al. [39] reported that the physiological folding of L1 requires the presence of Zn(II), although the number of zinc ions required for correct folding could not be ascertained. In the studies by Wommer et al. [38] in vitro metal binding studies with several MβLs showed that BcII and CphA exhibit vastly differing dissociation constants for 1-Zn and 2-Zn analogs. However, L1 and BlaB exhibit K_D values that are almost identical for the first and second zinc ions [38].

It is clear that the mono Zn forms of BcII and CphA may be physiologically relevant. The catalytic site in 1-Zn BcII is probably the Zn_1 site [40, 41], while the Zn_2 site is the catalytic site for the *Aeromonas* enzymes [42]. In the case of L1 and BlaB, it has yet to be established that a mononuclear Zn(II)-containing version of these enzymes can be prepared, given the relative K_D values [38]. With the ultimate goal of designing universal inhibitors that are effective against all MβLs, detailed information about the Zn(II) binding sites in these enzymes is critical. We report here the first preparation of a mononuclear version of MβL L1, and extended X-ray absorption fine structure (EXAFS) characterization of the 1-Zn and 2-Zn forms of L1. Data are also presented for an enzyme-bound product complex with nitrocefin.

Electronic Supplementary Material Supplementary material is available for this article at http://dx.doi.org/10.1007/s00775-006-0083-z and is accessible for authorized users.

A. Costello · D. L. Tierney (✉)
Department of Chemistry, University of New Mexico,
87131, Albuquerque, NM, Mexico
E-mail: dtierney@unm.edu
Tel.: +1-505-2772505
Fax: +1-505-2772609

G. Periyannan · K.-W. Yang · M. W. Crowder
Department of Chemistry and Biochemistry,
Miami University, Oxford, OH, 45056, USA

Materials and methods

L1 was overexpressed, purified, and made metal-free as described previously [43, 44]. Steady-state kinetics studies were conducted on 1-Zn and 2-Zn forms of L1, using previously defined methods [43]. All buffers were made metal-free by extensive treatment with Chelex-100 prior to use. Samples for EXAFS (approximately 1 mM in protein) were prepared with 20% (v/v) glycerol as a glassing agent. EXAFS samples were loaded in Lucite cuvettes with 6-μm polypropylene windows and frozen rapidly in liquid nitrogen. X-ray absorption spectra were measured at the National Synchrotron Light Source (NSLS), beamline X9B, with a Si(111) double-crystal monochromator; harmonic rejection was accomplished using a Ni focusing mirror. Fluorescence excitation spectra for all samples were measured with a 13-element solid-state Ge detector array. Samples were held at approximately 15 K in a Displex cryostat. EXAFS data collection and reduction were performed according to published procedures [45].

Data were measured in duplicate, on two samples from independent purifications; fits to the two data sets were equivalent. As both data sets gave similar results, the data were averaged; the experimental spectra presented here are the averaged data sets (12 scans per sample). The data were converted from energy to k-space using $E_0 = 9{,}680$ eV. Fourier-filtered EXAFS data were fit to Eq. 1, using the nonlinear least-squares engine of IFEFFIT that is distributed with SixPack (SixPack is available free of charge from http://www.sssrl.slac.stanford.edu/~swebb/index.html; IFEFFIT is open source software available from http://www.cars9.uchicago.edu/ifeffit):

$$\chi(k) = \sum \frac{N_{as} S_c}{k R_{as}^2} \exp\left(-2k^2\sigma_{as}^2\right) \exp\left(-2R_{as}/\lambda\right) \times \sin\left[2kR_{as} + \phi_{as}(k)\right]. \quad (1)$$

In Eq. 1, N_{as} is the number of scatterers within a given radius ($R_{as} \pm \sigma_{as}$), S_c is an absorber–scatterer (as) pair-dependent scale factor, $\phi_{as}(k)$ is the phase shift experienced by the photoelectron, λ is the photoelectron mean free-path, and the sum is taken over all shells of scattering atoms included in the fit. Theoretical amplitude and phase functions, $A_s(k)\exp(-2R_{as}/\lambda)$ and $\phi_{as}(k)$, were calculated using FEFF version 8.00 [46]. The Zn–N scale factor and the threshold energy, ΔE_0, were determined by fitting experimental data for tetrakis-1-methylimidazole zinc(II) perchlorate, $Zn(MeIm)_4$ [47]. The optimal values found were $S_c = 0.78$ and $\Delta E_0 = -21$ eV. Fits to L1 data were then obtained for all reasonable coordination numbers, holding S_c and ΔE_0 fixed, while varying R_{as} and σ_{as}^2. Fits to unfiltered data gave similar results.

Multiple-scattering contributions from histidine ligands were approximated by fitting FEFF calculated paths to the $Zn(MeIm)_4$ EXAFS [47]. The best fits resulted in four prominent multiple-scattering features, representing 140 total paths. Paths of similar overall length were combined to match these four prominent features. Consequently, no physical label can be meaningfully applied to these combined paths. Combined paths were used to fit the protein data, fixing the number of imidazole ligands per Zn ion at integral (or half-integral) values while varying R_{as} and σ_{as}^2. Metal–metal (Zn–Zn) scattering was modeled by fitting calculated amplitude and phase functions to the experimental EXAFS of $Zn_2(salpn)_2$.

Results

Addition of 1 equiv of Zn(II) to apo-L1 results in an enzyme that exhibits steady-state kinetics constants of $k_{cat} = 33 \pm 3\ s^{-1}$ and $K_m = 9 \pm 3$ μM when using nitrocefin as the substrate. These numbers are very similar to those of as-isolated L1 [43], which contains 1.9 equiv of Zn(II) ($k_{cat} = 38 \pm 1\ s^{-1}$; $K_m = 10 \pm 1$ μM). The addition of a second equivalent of zinc to 1-Zn L1 results in a k_{cat} value of $34 \pm 1\ s^{-1}$ and a K_m value of 5 ± 1 μM. While the buffers used in these studies were extensively treated with Chelex-100, it remains possible that nanomolar concentrations of free Zn(II) [38] were available to bind to 1-Zn L1. Thus, we cannot unambiguously rule out the possibility that the 1-Zn L1 used in the steady-state kinetics studies contained some amount of 2-Zn L1. However, this is unlikely to affect the spectroscopic studies, performed at millimolar concentrations, described later. With the preceding caveat, it appears that L1 is nearly fully active as a mononuclear enzyme, and the presence of a second zinc ion serves only to slightly increase the specificity (k_{cat}/K_m) of the enzyme. Clearly, this result demonstrates that the first equivalent of Zn(II) does not produce a mixture of fully loaded enzymes and apoenzymes, as this scenario would lead to 1-Zn L1 exhibiting a k_{cat} value that is half that of dinuclear 2-Zn L1. However, these results do not address whether the first equivalent of Zn(II) binds at the Zn_1 site, the Zn_2 site, or a site made up of metal binding amino acids from both sites.

To further probe Zn(II) binding, EXAFS spectra were collected for L1 containing 1 and 2 equiv of Zn(II). Experimental data, $k^3\chi(k)$, and the corresponding Fourier transforms (FT) are compared in Fig. 1. The FT for 1-Zn L1 shows an asymmetric first shell and three prominent peaks to higher R, consistent with the presence of multiple histidine ligands. The first-shell peak for 2-Zn L1 is significantly larger than for 1-Zn L1, indicating either an increase in coordination number or a decrease in disorder, or both, on addition of the second Zn(II). An added feature at $R + \alpha = 3.1$ Å is also apparent in the 2-Zn L1 FT, consistent with formation of a dinuclear cluster. Examination of the $k^3\chi(k)$ data shows a small phase shift from 1-Zn L1 to 2-Zn L1, especially notable at high k, where an additional frequency component can be identified for 2-Zn L1.

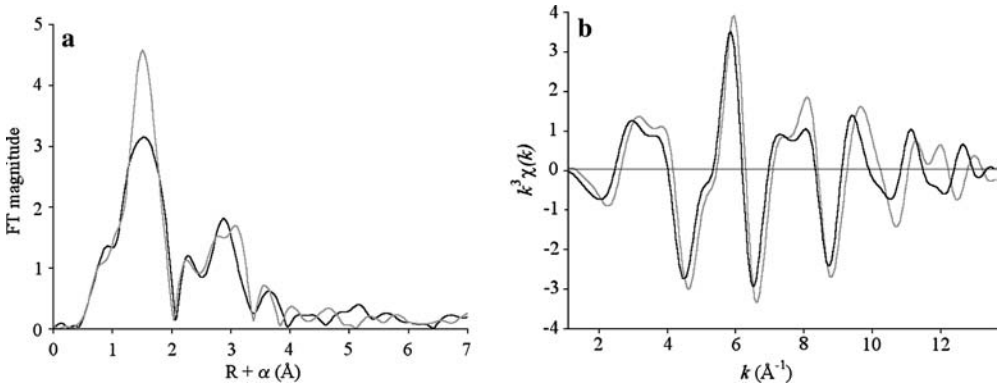

Fig. 1 Fourier transforms (**a**) of experimental k^3-weighted *EXAFS* data (**b**) for 1-Zn L1 (*black lines*) and 2-Zn L1 (*gray lines*)

Curve-fitting results are summarized in Table 1. Single-scattering fits to Fourier-filtered first-shell data for 1-Zn L1 show an average of four N/O scatterers (fit 1-1) at a distance of 2.03 Å. The first-shell fit is considerably improved (approximately 40%) by including separate contributions from one oxygen (1.91 Å) and three nitrogen (2.07 Å, fit 1-2) donors, consistent with the expected ligand set of the canonical Zn_1 site. Attempts to fit the data with a model derived from homogeneous occupation of the Zn_2 site, or from equal occupancy of the Zn_1 and Zn_2 sites, led to refined Zn–O and Zn–N distances that cannot be resolved with the current data, which affords a resolution of approximately 0.13 Å. In addition, the fit residuals were nearly a factor of 2 larger than the model for occupation of the Zn_1 site (see Table S1, compare fits S2–S4 and S5–S7). The multiple-scattering fit shown in Fig. 2 is the sum of first-shell, single-scattering contributions (1O, 3N) and three (±0.5) rigid imidazole rings (fit 1–3). The value of σ_{as}^2 for the outer shells increases monotonically, owing to the increasing spread in path length and the number of scattering legs in the combined paths. Inclusion of a Zn–Zn interaction (Table S1) does not improve the fit residual.

For 2-Zn L1, first-shell fits also show an average of four N/O scatterers per zinc ion at a distance of 2.01 Å (Table 1, fit 2–1). Two distinct first-shell interactions could not be resolved, the best fit giving an average of two oxygens at 1.97 Å and two nitrogens at 2.03 Å (fit 2–2). The slight reduction in average bond length most

Table 1 Extended X-ray absorption fine structure (*EXAFS*) curve-fitting results for 1-Zn and 2-Zn L1, and 2-Zn L1 + nitrocefin

	Model	Zn–O	Zn–N	Zn–S	Zn–His[a]		Zn–Zn	R_f[b]	R_u
1-Zn L1									
1–1	4N/O		2.03 (5.9)					55	289
1–2	1O + 3N	1.91 (2.3)	2.07 (2.0)					33	277
1–3	1O + 3 N + 3His	1.91 (4.0)	2.07 (2.5)		2.97 (4) 3.62 (14)	3.24 (1) 4.50 (20)		32	79
2-Zn L1									
2–1	4 N/O		2.01 (4.6)					19	235
2–2	1O + 3 N	1.97 (1.5)	2.03 (2.4)					14	229
2–3	1O + 3 N + 2.5 His	1.97 (2.8)	2.03 (2.7)		2.92 (3) 4.03 (13)	3.17 (2) 4.46 (18)		130[c]	81
2–4	1O + 3 N + 2.5 His + Zn–Zn	1.97 (1.7)	2.03 (2.5)		2.89 (3) 4.00 (29)	3.13 (1) 4.44 (18)	3.42 (5.3)	39	50
2-Zn L1 + nitrocefin									
3–1	4.5 N/O		2.05 (3.9)					90	266
3–2	1.5O + 3N	1.93 (0)	2.07 (1.3)					69	264
3–3	4N + 0.5S	2.04 (4.1)		2.29 (4.2)				22	155
3–4	4N + 0.5S + 2.5 His	2.03 (4.1)		2.29 (4.0)	2.92 (7) 4.16 (16)	3.15 (5) 4.49 (22)		42	54
3–4	4N + 0.5S + 2.5 His + Zn–Zn	2.04 (4.0)		2.29 (4.3)	2.94 (9) 4.08 (14)	3.23 (14) 4.50 (26)	3.62 (6.1)	24	33

Distances (angstroms) and Debye–Waller factors (σ^2 in units of 10^{-3} Å^2, in *parentheses*) derive from integer or half-integer coordination number fits to filtered EXAFS data: $\Delta k = 1.1$–12.8 Å^{-1}; $\Delta R = 0.5$–2.1 Å for first-shell fits, $\Delta R = 0.1$–4.5 Å for multiple-scattering fits

[a]Multiple-scattering paths represent the combined paths described in the "Materials and methods"

[b]Goodness of fit (R_f for fits to filtered data, R_u for fits to unfiltered data) defined as $1,000 \times \sum_{i=1}^{N} \left(\chi_{i_{calc}} / \chi_{i_{obs}}\right)^2$, where N is the number of data points

[c]The larger residual for the filtered fit, relative to the unfiltered fit, is an artifact of the Fourier filtering process, which converts real data (unfiltered) into complex data (filtered). This results in an effective doubling of the number of points being fit, and will on occasion (particularly for high-quality raw data) lead to a higher residual for fits to filtered data

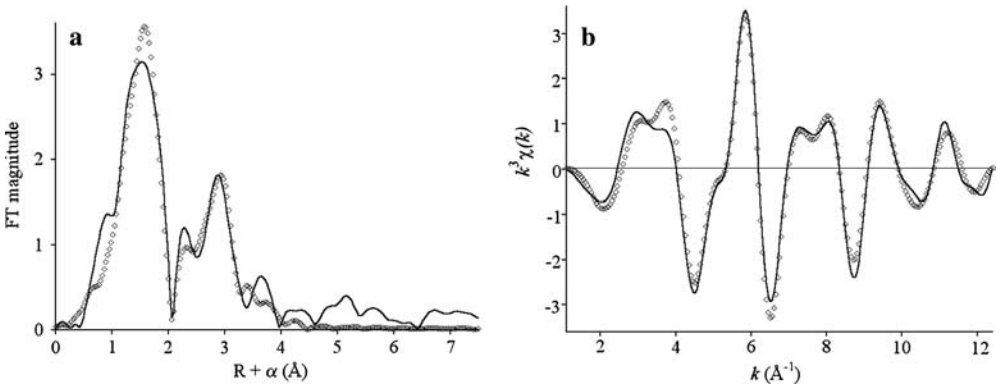

Fig. 2 Fourier transforms (**a**) of experimental k^3-weighted EXAFS data (**b**) for 1-Zn L1 (*black lines*) and the best fit (*open diamonds*), including a first shell of one O and three N donors, and multiple scattering from three histidine imidazoles

likely reflects an increase in the amount of O (vs. N) donation in the first shell. Multiple-scattering fits that include four N/O in the first shell and 2.5 histidines per zinc ion match the majority of the features in the FT (fit 2–3; Fig. 3a, top), with the exception of the extra component, noted before, at $R+\alpha = 3.1$ Å, and poor reproduction of the outermost feature in the data. Inspection of the fit in *k*-space (Fig. 3b, top) shows an inadequate fit to the first, third, and fifth oscillations. Addition of a Zn–C interaction at approximately 3 Å, to simulate carboxylate carbon scattering, did not improve the fit. In contrast, addition of a Zn–Zn interaction substantially improves the appearance of the fit, nicely duplicating the outer-shell features in *R*-space (Fig. 3a, bottom) and the shoulders at $k\sim3.8$, 7.4, and 11 in *k*-space (Fig. 3b, bottom). The quantitative improvement in the fit is dramatic, with a 70% decrease in the fit residual (compare fits 2–3 and 2–4). The refined Zn–Zn distance of 3.42 Å is in excellent agreement with that reported in the crystal structure (3.4 Å) [48].

To interrogate the interaction of substrates with the dinuclear cluster of L1, the enzyme–product complex of L1 with hydrolyzed nitrocefin (1:1) was examined. Comparison of the EXAFS and the corresponding FTs for 2-Zn L1 (resting state) and 2-Zn L1 + nitrocefin (enzyme–product complex, Fig. 4), shows several significant changes, including an apparent phase shift in the principal frequency (shift to higher *R* of the main peak in Fig. 4a). This phase shift is readily apparent in the *k*-space data (Fig. 4b). The marked increase in intensity of the main peak may be reflective of lower disorder, an increase in coordination number, or perhaps the addition of one or more higher-*Z* ligands. The outer-shell scattering is also altered, with an obvious change in the feature previously ascribed to the Zn–Zn interaction in resting 2-Zn L1.

Fits to the 2-Zn L1 + nitrocefin data indicate that the increased intensity of the main peak in the FT can be attributed, in part, to the addition of a sulfur ligand to one of the Zn ions. The disorder in the low-*Z* component of the first shell is also reduced in the product complex (Table 1, fits 3–1 to 3–3). While a mixed low-*Z* shell of 1.5 N and three O leads to a marginal improvement in the fit (approximately 23%, fits 3–1 and 3–2), the inclusion of a single sulfur scatterer, averaged over the two Zn ions, leads to nearly fourfold improvement in the fit residual (compare fits 3–1 and 3–3). Multiple-scattering fits, including a first shell of four low-*Z* (N/O) scatterers and 0.5 S per zinc ion, with varying numbers of imidazolate ligands, indicate 2.5 histidine ligands per zinc, similar to resting 2-Zn L1. Addition of a Zn–Zn interaction leads to a substantial improvement in the fit (43%, Fig. 5). The Zn–Zn distance increases to 3.62 Å in the product complex, requiring that the bound product bridge the two Zn ions.

To match the lower amplitude of the histidine scattering for the product complex, multiple-scattering fits refine to slightly elevated disorder parameters for the

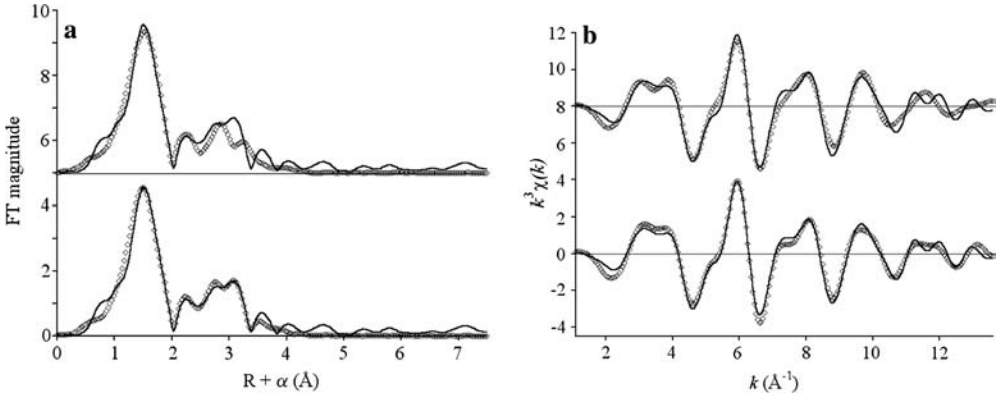

Fig. 3 Fourier transforms (**a**) of experimental k^3-weighted EXAFS data (**b**) for 2-Zn L1 (*black lines*) and the best fits (*open diamonds*). *Top*: Multiple scattering fit including one O and three N first-shell donors, with 2.5 imidazoles per zinc ion. *Bottom*: Multiple-scattering fit including one O and three N in the first shell, with 2.5 imidazoles per Zn ion, and a Zn–Zn interaction at 3.42 Å. The data have been offset vertically for clarity

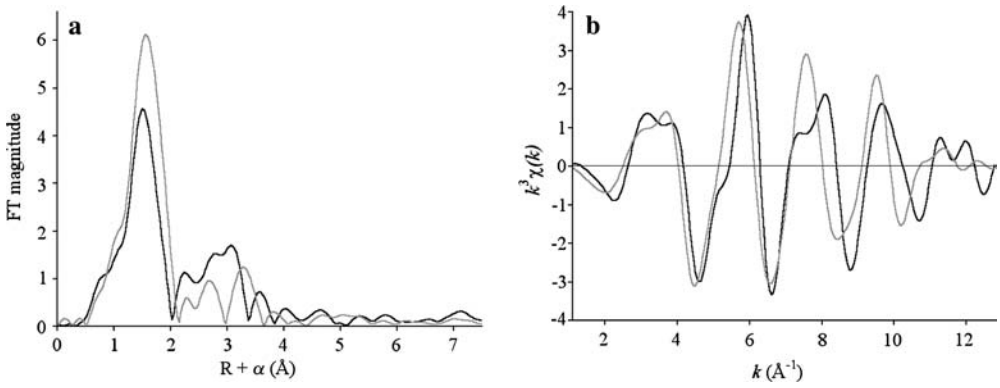

Fig. 4 Comparison of Fourier transforms (**a**) of k^3-weighted EXAFS (**b**) for 2-Zn L1 (*black lines*) and 2-Zn L1 + nitrocefin (*gray lines*)

outer shells (Table 1, fit 3–3). This lower amplitude is most likely an artifact of destructive interference from the Zn–S scattering, which passes in and out of phase with the Zn–His scattering (at roughly twice the frequency), and from the Zn–Zn scattering, which is out of phase with the Zn–His scattering over most of the available *k*-range. Additionally, the bridging hydrolyzed product is expected to give rise to minor outer-shell scattering, the features of which have not been included in the model. These may also serve to reduce the apparent histidine-scattering amplitude. Individual contributions to the fit in Fig. 5 are plotted separately in Fig. S1.

Discussion

Sequential metal binding

Kinetics analyses indicate that the first equivalent of Zn(II) binds to only one well-defined site. As a mononuclear zinc enzyme, L1 appears to be nearly fully active. The second zinc ion tunes the specificity (k_{cat}/K_m) of the enzyme. The kinetics constants reported here are dramatically different from those measured for the same enzyme with imipenem as the substrate [38], most likely reflecting the difference in L1's ability to hydrolyze cephalosporins (nitrocefin) versus carbapenems (imipenem) [43]. The kinetics results are inconsistent with the first equivalent of Zn(II) producing a mixture of fully loaded enzymes and apoenzymes, as this would predict a k_{cat} value for 1-Zn L1 that is half that of 2-Zn L1. These results do not address whether the first equivalent of zinc binds at the Zn_1 site, the Zn_2 site, or at a site that contains metal binding amino acids from both.

Garrity et al. [31] recently showed that the fluorescence properties of L1 could be attributed to one tryptophan in the enzyme (W39). The stoichiometry of fluorescence titrations (fluorescence ceases to increase at approximately 0.9 Zn per monomer, with no change in fluorescence above 1 equiv of Zn) clearly indicates sequential metal binding by L1, and disqualifies the notion of Zn occupying both sides of the active site, as this would require that the fluorescence increase monotonically up to 2 equiv of zinc. This is in contrast to previous studies on the B1 lactamase BcII from *B. cereus* [49]. Given the proximity of W39 to metal binding His263 [48], it was suggested that the first equivalent of zinc selectively binds at the Zn_2 site [31]. However, the possibility remains that binding of the second Zn ion does not change the position of His263 (nor the fluorescence of W39). In this case, Zn(II)-bound water would interact, through Asp120, with the NH of His 263, and an edge His263/face Trp39 interaction would be responsible for the fluorescence. This, in effect, would require some pre-arrangement of the ligands at the Zn_2 site on binding metal at the Zn_1 site.

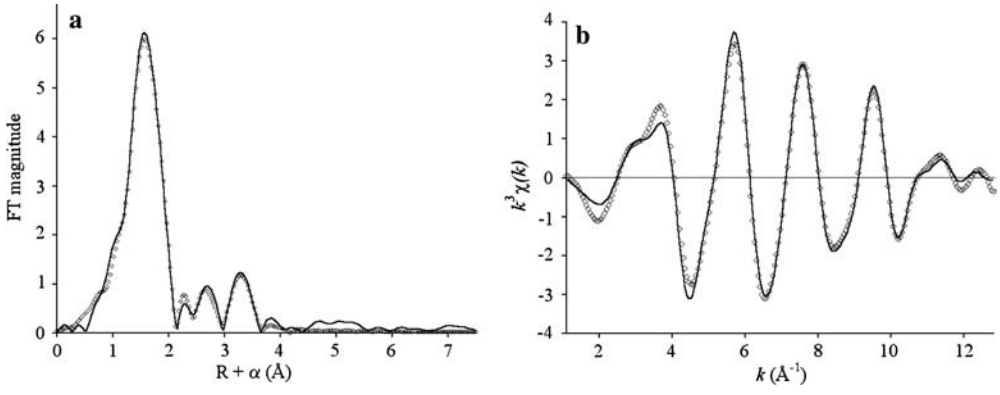

Fig. 5 Fourier transforms (**a**) of experimental k^3-weighted EXAFS data (**b**) for 2-Zn L1 + nitrocefin (*black lines*) and the best fit (*open diamonds*)

The EXAFS data presented here (Fig. 1) favor binding of the first equivalent of metal at the Zn_1 site. Although the relative number of histidine ligands in 1-Zn L1 and 2-Zn L1 is difficult to distinguish, the data are significantly better determined for 1-Zn L1, without the additional Zn–Zn contribution to the EXAFS, and the curve-fitting results clearly indicate binding at the Zn_1 site. We believe the decrease in average first-shell bond length from 1-Zn L1 to 2-Zn L1 lends further support to this interpretation. According to the crystal structure of the enzyme [48], Zn in the Zn_1 site will be four-coordinate and Zn in the Zn_2 site will be five-coordinate. If Zn_1 is loaded first, the average coordination number should increase from 4 to 4.5 on addition of the second metal ion. The minimal effect of this increase in coordination number on the average bond length can easily be compensated by the increased oxygen content of the first shell (from 25 to 33%). Further support for this conclusion is given in the following.

While binding of the first metal ion results in a homogeneous, well-ordered active site, the EXAFS data indicate the binding of the second metal ion organizes the primary coordination sphere of the two Zn ions, without significant rearrangement of the first site. The increased amplitude of the first shell peak for 2-Zn L1 (Fig. 1) cannot be explained by the expected increase in coordination number (from 4 to 4.5), and slightly lower disorder is reflected in the fits (Table 1, fits 1–1 and 2–1). An alternative explanation is that the second metal site itself is intrinsically more ordered than the first. This is consistent with the suggestion earlier that binding of the first metal organizes the ligand set of the Zn_2 site (His263 and Asp120, suggested by the fluorescence properties of W39) [31], minimizing rearrangement on incorporation of the second metal ion. Control of metal binding in this manner would further support the conclusion that the first equivalent of Zn(II) binds at the Zn_1 site.

The enzyme-product complex

The EXAFS data on the product complex offer two significant observations. The first is that the enzyme-bound product bridges the two metal ions. This is in contrast to earlier studies on the interaction of di-Co L1 with nitrocefin [50], which suggested, based on an apparent lack of magnetic coupling, that the bound product did not bridge the metal ions. It is, however, consistent with recent crystallographic results for this enzyme with hydrolyzed moxalactam [34]. The lengthening of the metal–metal interaction seen here, from 3.42 to 3.62 Å, is the same as that seen with moxalactam and must be imposed by the bound product species, requiring intimate interaction with both metal ions. The possibility remains that the di-Co form of the enzyme does not bind product in the same manner as the di-Zn enzyme.

Perhaps more intriguing is the addition of a sulfur ligand in the product complex. This observation requires that the ring-opened lactam rotate (about the C6–C7 bond, Fig. 6) in the active site in order for the sulfur atom to gain close enough approach to coordinate. The current data, however, cannot comment on either the orientation of the bound product (i.e., which metal coordinates the sulfur atom) or on which group coordinates the other metal ion. One possibility is that the product remains coordinated to one Zn, through, for example, the newly formed carboxylate (at C8) generated in the hydrolysis reaction, and the other half of the product rotates about the C6–C7 single bond that was formerly part of the four-membered lactam ring. It is also possible that the entire product dissociates, rotates, and recoordinates, retaining its original orientation. It is unlikely that EXAFS alone will be able to answer this question.

It is also unclear whether the bridging solvent molecule is retained in the nitrocefin product complex. The metal–metal distance in the product complex is sufficiently short to accommodate the presence of a second bridge. Retention of the solvent bridge would force the $Zn–OH_x–Zn$ interaction to be nearly linear, which should amplify the metal–metal EXAFS; no evidence for such amplification is apparent, suggesting the solvent bridge may be lost. This is consistent with the first-shell fits presented here and the previous studies on di-Co L1 [50], which suggest that the coordination number of Zn_1 does not change on formation of the product complex.

Comparison of the present EXAFS data with the crystal structure of L1 complexed with hydrolyzed moxalactam [34] offers some important similarities, and some intriguing differences. Both studies show that the hydrolyzed product coordinates the two metal ions simultaneously. However, while the increase in metal–metal distance is the same for both substrates, this appears to be fortuitous, as the two products appear to coordinate differently. Some of these differences can be

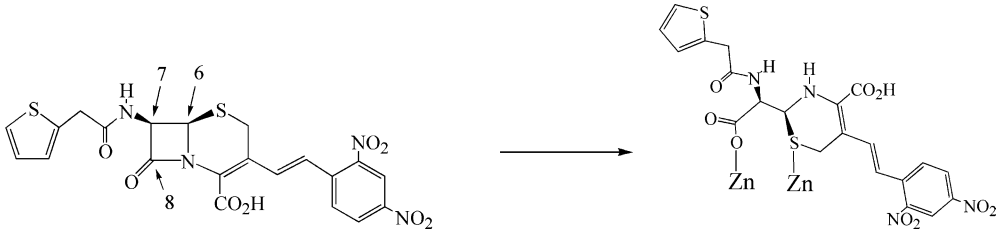

Fig. 6 Orientation of hydrolyzed nitrocefin and potential contacts with zinc ions in the L1 active site

accounted for by comparing the structures of nitrocefin and moxalactam (Scheme 1).

Scheme 1

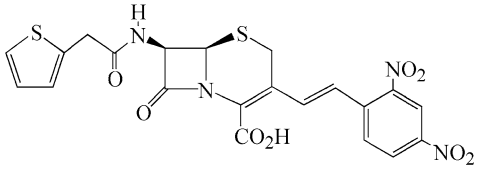

nitrocefin

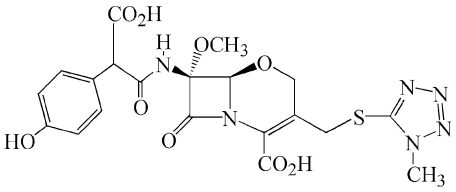

moxalactam

The crystal structure with moxalactam shows interaction of an anionic lactam nitrogen and the 4-carboxylate with Zn_2; the newly formed C8 carboxylate coordinates Zn_1. Retention of the bridging solvent is facilitated by interaction with the C7 methoxy group, which requires rotation of the product species in the active site, about the C6–C7 single bond. In this model, both metals gain ligands from the bound product, and the average coordination number of the two Zn ions increases from 4.5 to 5.5. A concomitant increase in average bond length of approximately 0.1 Å is also observed. The Zn–O distances to the bridging solvent molecule also increase by approximately 0.1 Å, suggesting perhaps a water molecule in the bridging position in the product complex, with hydroxide occupying this position in the resting enzyme. The increase in bond length may also indicate a transition from bridging to terminal on one zinc ion. It remains unclear whether these results are truly conflicting.

The present EXAFS studies of the nitrocefin complex also indicate rotation of the bound product about the C6–C7 single bond. However, in the nitrocefin complex, this rotation results in coordination of the sulfur atom. This requires that the lactam nitrogen (N5) be released, in turn requiring its protonation. It also requires that the C4 carboxylate no longer coordinates. There is no group in nitrocefin analogous to the C6 methoxy to help stabilize retention of the bridging solvent, which we propose is absent in the nitrocefin complex. Loss of the solvent bridge in the nitrocefin complex would maintain an average coordination number of 4.5 for the two Zn ions, consistent with the lack of an appreciable change in average first-shell bond length in the present EXAFS studies. The differences in product binding may reflect differences in orientation of the substrates in the pocket (i.e., rotated 180° with respect to each other), or in the final product structures, where the thiotetrazole is lost on hydrolysis of moxalactam, while the dinitrophenyl moiety is retained in hydrolyzed nitrocefin. It is possible that nonfavorable interaction of the dinitrophenyl with the surrounding protein is responsible for the rotation of nitrocefin.

Conclusion

The EXAFS studies presented here indicate that the first, catalytically dominant metal ion is bound by L1 at the consensus Zn_1 site. The data further suggest that binding of the first metal helps preorganize the ligands for binding of the second metal ion. Reaction with the β-lactam antibiotic nitrocefin results in a bridging product-bound species, in which the ring-opened lactam rotates in the active site to present the sulfur atom to one of the metal ions for coordination.

Acknowledgements Financial support for this work was provided by the National Institutes of Health (P20RR-16480 from the BRIN/INBRE Program of the National Center for Research Resources to D.L.T. and GM40052 to M.W.C.). The National Synchrotron Light Source is supported by the US Department of Energy.

References

1. Cricco JA, Orellano EG, Rasia RM, Ceccarelli EA, Vila AJ (1999) Coord Chem Rev 190–192:519–535
2. Crowder MW, Walsh TR (1999) Res Signpost 3:105–132
3. Heinz U, Adolph HW (2004) CMLS Cell Mol Life Sci 61:2827–2839
4. Wang Z, Fast W, Valentine AM, Benkovic SJ (1999) Curr Opin Chem Biol 3:614–622
5. Materon IC, Queenan AM, Koehler TM, Bush K, Palzkill T (2003) Antimicrob Agents Chemother 47:2040–2042
6. Concha NO, Janson CA, Rowling P, Pearson S, Cheever CA, Clarke BP, Lewis C, Galleni M, Frere JM, Payne DJ, Bateson JH, Abdel-Meguid SS (2000) Biochemistry 39:4288–4298
7. Wang Z, Fast W, Benkovic SJ (1998) J Am Chem Soc 120:10788–10789
8. Wang Z, Fast W, Benkovic SJ (1999) Biochemistry 38:10013–10023
9. Fast W, Wang Z, Benkovic SJ (2001) Biochemistry 40:1640–1650
10. Diaz N, Suarez D, Merz KM (2000) J Am Chem Soc 122:4197–4208
11. Yanchak MP, Taylor RA, Crowder MW (2000) Biochemistry 39:11330–11339
12. Salsbury FR, Crowley MF, Brooks CL (2001) Protein Struct Funct Genet 44:448–459
13. Suarez D, Brothers EN, Merz KM (2002) Biochemistry 41:6615–6630
14. Suarez D, Diaz N, Merz KM (2002) J Comput Chem 23:1587–1600
15. Suarez D, Merz KM (2001) J Am Chem Soc 123:3759–3770
16. Krauss M, Gresh N, Antony J (2003) J Phys Chem B 107:1215–1229
17. Bicknell R, Emanuel EL, Gagnon J, Waley SG (1985) Biochem J 229:791–797

18. Bicknell R, V. Knott-Hunziker; Waley SG (1983) Biochem J 213:61–66
19. Bicknell R, Schaffer A, Waley SG, Auld DS (1986) Biochemistry 25:7208–7215
20. Diaz N, Suarez D, Merz KM (2001) J Am Chem Soc 123:9867–9879
21. Bounaga S, Laws AP, Galleni M, Page MI (1998) Biochem J 331:703–711
22. Hemmingsen L, Damblon C, Antony J, Jensen N, Adolph HW, Wommer S, Roberts GCK, Bauer R (2001) J Am Chem Soc 123:10329–10335
23. Moali C, Anne C, Lamotte-Brasseur J, Groslambert S, Devreese B, Van Beeumen J, Galleni M, Frere JM (2003) Chem Biol 10:319–329
24. Dal Peraro M, Vila AJ, Carloni P (2004) Proteins Struct Funct Bioinformat 54:412–423
25. Estiu GL, Rasia RM, Cricco JA, Vila AJ, Zerner MC (2002) Int J Quantum Chem 88:118–132
26. Oelschlaeger P, Schmid RD, Pleiss J (2003) Protein Eng 16:341–350
27. Oelschlaeger P, Schmid RD, Pleiss J (2003) Biochemistry 42:8945–8956
28. Haruta S, Yamamoto ET, Eriguchi Y, Sawai T (2001) FEMS Microbiol Lett 197:85–89
29. Carenbauer AL, Garrity JA, Periyannan G, Yates RB, Crowder MW (2002) BMC Biochem 3:4–10
30. Garrity JD, Carenbauer AL, Herron LR, Crowder MW (2004) J Biol Chem 279:920–927
31. Garrity JD, Pauff JM, Crowder MW (2004) J Biol Chem 279:39663–39670
32. S. McManus-Munoz, Crowder MW (1999) Biochemistry 38:1547–1553
33. Spencer J, Clark AR, Walsh TR (2001) J Biol Chem 276:33638–33644
34. Spencer J, Read J, Sessions RB, Howell S, Blackburn GM, Gamblin SJ (2005) J Am Chem Soc 127:14439–14444
35. Cricco JA, Vila AJ (1999) Curr Pharm Des 5:915–927
36. Vallardes MH, Feilici A, Weber G, Adolph HW, Zeppezauer M, Rossolini GM, Amicosante G, Frere JM, Galleni M (1997) Biochemistry 36:11534–11541
37. Crawford PA, Sharma N, Chandrasekar S, Sigdel T, Walsh TR, Spencer J, Crowder MW (2004) Prot Express Purif 36:272–279
38. Wommer S, Rival S, Heinz U, Galleni M, Frere JM, Franceschini N, Amicosante G, Rasmussen B, Bauer R, Adolph HW (2002) J Biol Chem 277:24142–24147
39. Periyannan G, Shaw PJ, Sigdel T, Crowder MW (2004) Protein Sci 13:2236–2243
40. Carfi A, Pares S, Duee E, Galleni M, Duez C, Frere JM, Dideberg O (1995) EMBO J 14:4914–4921
41. Orellano EG, Giardini JE, Cricco JA, Vila AJ (1998) Biochemistry 37:10173–10180
42. Crawford PA, Yang KW, Sharma N, Bennett B, Crowder MW (2005) Biochemistry 44:5168–5176
43. Crowder MW, Walsh TR, Banovic L, Pettit M, Spencer J (1998) Antimicrob Agents Chemother 42:921–926
44. Crowder MW, Yang K-W, Carenbauer AL, Periyannan G, Seifert ME, Rude NE, Walsh TR (2001) J Biol Inorg Chem 6:91–99
45. Thomas PW, Stone EM, Costello AL, Tierney DL, Fast W (2005) Biochemistry 44:7559–7565
46. Ankudinov AL, Ravel B, Rehr JJ, Conradson SD (1998) Phys Rev B 58:7565–7576
47. McClure CP, Rusche KM, Peariso K, Jackman JE, Fierke CA, Penner-Hahn JE (2003) J Inorg Biochem 94:78–85
48. Ullah JH, Walsh TR, Taylor IA, Emery DC, Verma CS, Gamblin SJ, Spenser J (1998) J Mol Biol 287:125–136
49. de Seny D, Heinz U, Wommer S, Kiefer M, Meyer-Klaucke W, Galleni M, Frere JM, Bauer R, Adolph HW (2001) J Biol Chem 276:45065–45078
50. Garrity JD, Bennett B, Crowder MW (2005) Biochemistry 44:1078–1087